# Sustainable Earth Review

# The impact of seasonal vegetation changes on retention and yield of sediment across the Tajan watershed in Sari, northern Iran

Mohammad Rahmani[*a] 🆔, Fazlolah Ahmadi Mirghaed[a], Sareh Molla Aghajanzadeh[a]

[a] Department of Environmental Sciences, Faculty of Marine and Environmental Sciences, University of Mazandaran, Babolsar, Iran

**A B S T R A C T**

Sediment retention (SR) and sediment yield (SY) are regulatory ecosystem services that would change due to seasonal vegetation conditions in a region. This study aimed to investigate the SR and SY in the Tajan watershed in Mazandaran Province, northern Iran, and their relationships to seasonal vegetation changes during 2022. The sediment delivery ratio model was implemented to evaluate SR and SY for four seasons using the InVEST software. Their relationship with the vegetation indices was also evaluated using geographically weighted regression (GWR) in Arc GIS 10.7. The highest level of SR and SY was observed in the central and southern parts of the watershed, respectively. The total SR and SY were estimated at 229 Mt y$^{-1}$ (471 t ha$^{-1}$ y$^{-1}$ on average) and 5.2 Mt y$^{-1}$ (11 t ha$^{-1}$ y$^{-1}$ on average), respectively. The maximum and minimum of SR occurred in the spring and winter, respectively, whereas the opposite was true for SY. Regional forests retained the most sediment, whereas rangelands had the highest SY. The GWR results showed a significant and positive geographic correlation between SR and vegetation indices ($0.76 < R^2 < 0.84$, P-value$<0.01$) but an inverse correlation between SY and vegetation indices ($0.67 < R^2 < 0.85$, P-value$<0.01$). Temporally, the highest geographic correlation of SR to the vegetation indices was seen in the summer, whereas the highest geographic correlation of SY to the vegetation indices was related to the winter. The results suggested that seasonal vegetation changes in the region could have a wide range of effects on the retention and yield of sediment. This study offers valuable insights for identifying areas of significant erosion throughout the watershed, during different seasons. Such information can aid managers and planners in adopting effective strategies to conserve soil and reduce erosion.

**A R T I C L E I N F O**

## 1. Introduction

Natural ecosystems can provide various services to humans either directly or indirectly (MEA, 2005). Certain ecosystem services, such as food, water, air, and fuel, benefit humans directly, whereas others, such as carbon sequestration, climate control, biodiversity, aesthetic value, and soil retention, indirectly affect the lives of humans and other species (MEA, 2005; Sharp et al., 2020). Ecosystem services can be seriously affected by natural and anthropogenic processes. Two of the most important processes, erosion and sedimentation, are regarded as major environmental issues worldwide.

Various factors such as human activity, land use conversion, climate change, and agricultural development intensify these processes, consequently, leading to deterioration of water quality, increase of mud in water reservoirs, and affecting the health of ecosystems and various ecosystem services such as sediment retention and yield (Hendi et al., 2022; Tikuye et al., 2023; Woznicki et al., 2020; Zhang et al., 2021). Sediment retention (SR) and sediment yield (SY) are regulatory ecosystem services that represent the capacity of regional vegetation to prevent erosion. Increasing SR and decreasing SY while preserving soil fertility results in lower dredging costs in downstream areas (Bagdon et al., 2016; Fan et al., 2016).

SR and SY are largely influenced by changes in land use and climate. The interaction between climate, land use, and vegetation is among the most important factors affecting SR and SY (Fenta et al., 2021; Polasky et al., 2012; Tikuye et al., 2023). Nonetheless, vegetation could be more important for retaining sediments and reducing erosion. Preserving vegetation in highly erodible sites results in greater retention of sediments and soil nutrients preventing erosion and its consequences, such as eutrophication and pollution of downstream areas. Moreover, the heterogeneity of topography, soil property, and landform of ecosystems and their effects on certain ecological criteria, such as precipitation, temperature, evapotranspiration, soil texture, soil water retention and soil permeability can affect environmental conditions regarding erosion and sedimentation (Betrie et al., 2011; Fan et al., 2018; Hirave et al., 2023; Zhou et al., 2021). Many models and instruments have been developed for evaluating SY and SR. Wischmeier and Smith (1978) proposed the first empirical method entitled Universal Soil Loss Equation (USLE), which was later modified into the Revised Universal Soil Loss Equation (RUSLE). RUSLE is also regarded by researchers as an evaluation model for SR and SY in the integrated valuation of ecosystem services and trade-offs (InVEST) software. Developed by the Natural Capital Project, InVEST is a tool for evaluating and mapping different ecosystem services (Sharp et al., 2020). Many scholars around the world have used this tool in the last decade to assess various ecosystem services including sediment retention and soil erosion (da Cunha et al., 2022; Gashaw et al., 2021; Tikuye et al., 2023), water yield (Daneshi et al., 2021; Li et al., 2021), nutrient retention (Hou et al., 2020; Redhead et al., 2018), carbon sequestration (Babbar et al., 2021; Saha et al., 2022), and habitat quality (Bastos et al., 2023; Wei et al., 2022). The advantages of this open-source tool include availability, user-friendliness, limited data requirements, ease of use, and acceptable results. Tikuye et al. (2023) used InVEST to model sediment and nutrient retention in the basin of Lake Tana, Ethiopia, and measure their changes based on the effects of land use and climate changes over 30 years. They confirmed that combining geographic data in InVEST can be helpful for land use planning, making decisions about nutrient and sediment export

control, and prioritizing basin management. Mirghaed and Souri (2023) applied InVEST to evaluate SR and SY in the Shoor River basin, Khuzestan Province of Iran. They found that the region's mean annual SR and SY were 13.3 t ha$^{-1}$y$^{-1}$ and 2.7 t ha$^{-1}$y$^{-1}$, respectively. Zhou et al. (2021) combined the RUSLE with the sediment delivery ratio (SDR) model to evaluate the dynamics of SR under socioeconomic development and environmental protection policies and determined the share of specific ecological and socioeconomic drivers in this regard. Woznicki et al. (2020) employed physiographic and remote sensing data in the RUSLE model to investigate SR in the US. Their findings indicated that soil retention is a function of physiography and varies geographically, whereas natural vegetation prevents annual sediment export to waterbodies. Several studies have investigated the retention and yield of sediment and their relationship with changes in land use and climate, vegetation, and topographic features. However, the effect of seasonal vegetation changes on SY and SR, especially in Iran, has rarely been addressed. Vegetation exerts a significant effect on SR and SY. By covering the soil surface, reducing the kinetic energy of raindrops, and preventing the direct impact of raindrops on the soil, vegetation canopy reduces the amount of soil carried by runoff, thereby decreasing soil particle movement and erosion (Shi et al., 2022; Wei et al., 2024; Zuazo et al., 2008). However, spatiotemporal alteration of vegetation can affect its contribution to mitigating soil erosion and enhancing soil conservation. This study hence examines the effect of seasonal vegetation changes on SR and SY in the Tajan watershed in northern Iran in 2022. The main objectives were as follows: (i) Using InVEST to model the ecosystem services of SR and SY in the study area, (ii) Investigating the effect of seasonal vegetation changes on SR and SY, (iii) Examining the relationship of vegetation indices with SR and SY in different seasons, and (iv) Evaluating changes of SR and SY in different land uses in four seasons during 2022.

## 2. Material and Methods

### 2.1. Study area

With an estimated area of 472,000 ha, Tajan is one of Iran's most important watersheds in

Mazandaran Province, north of Iran (Fig. 1). This region has an average altitude of 1,179 m above sea level, an average annual precipitation of 640 mm and an average annual temperature of 25°C. The minimum and maximum monthly rainfall of the region (equal to 33.5 mm and 69.4 mm, respectively) are reported in July and November (Regional Water Company of Mazandaran, 2023). Geomorphologically, the watershed has two dominant landforms, namely mountainous and plain. Over 60% of the region is mountainous, 25% is plains and coastal plains, and the remaining 5% is fluvial terraces, foothills, and hills. The majority of the Tajan watershed is covered by forests and rangelands, particularly in the mountains, while the plains to the region's north are allocated to agriculture and built-up environments. The rivers originate from the region's southern heights and pass-through mountainous areas and coastal plains to finally flow into the Caspian Sea. With a population of over 500,000 people, the city of Sari is the most important population center in this watershed.
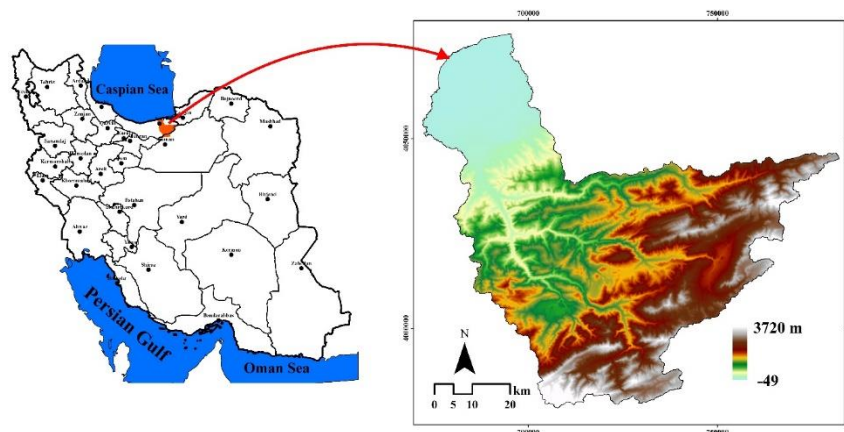


**Fig. 1.** Geographical location of the Tajan watershed

### 2.2. Data Preparation

The land use map of the study area was produced based on Landsat 8 satellite images (path 165 and row 35, 30/06/2022) using the support vector machine (SVM) method in the ENVI 5.3 software. Obtained from the Shuttle Radar Topography Mission (SRTM) images, the digital elevation model (DEM) was inserted into the InVEST software to calculate slope length and gradient (LS factor). Mean annual and monthly precipitation data were received from statistics by the region's meteorological stations and used to estimate the Fournier index and rainfall erosivity (R factor) according to equations 1 and 2. The maps of clay, sand, silt, and soil organic carbon were acquired from the ISRIC images in the Google Earth Engine and utilized to assess the soil erodibility (K factor) using equation 3. The land cover management factor (C factor) was derived from the normalized difference vegetation index (NDVI) using equation 4. The land management and conservation factor (P factor) was determined according to slope map classification (Table 1) and calculation of its average for each land use. Vegetation index maps including NDVI, soil-adjusted vegetation index (SAVI), enhanced vegetation index (EVI), and leaf area index (LAI) were prepared based on surface reflectance images from the Landsat 8 satellite in the Google Earth Engine for all four seasons of 2022. These indices were calculated using equations 5 to 8, respectively. The sub-watershed map was also generated in the Arc GIS 10.7 software using the region's DEM.

$$F = \sum_{i=1}^{12} p_i^2 / Pr \tag{1}$$

$$R = \begin{cases} (0.07397F^{1.847}) & if \quad F < 55\ mm \\ (95.77 - 6.081F + 0.477F^2) & if \quad F \geq 55\ mm \end{cases} \tag{2}$$

$$K = \left(0.2 + 0.3exp\left[-0.0256SA\frac{(1-SI)}{100}\right]\right)\left(\frac{SI}{CL+SI}\right)^{0.3}\left(1.0 - \frac{0.25OC}{OC+\exp(3.72+2.90OC)}\right)\left(1.0 - \frac{0.7(1-\frac{SA}{100})}{(1-\frac{SA}{100})+\exp(-5.51+22.9(1-\frac{SA}{100}))}\right) \tag{3}$$

$$C = exp[-\alpha(NDVI/\beta - NDVI)] \tag{4}$$

where $F$, $p_i$, $P_r$, and $R$ denote the Fournier index, average monthly precipitation (mm), average annual precipitation (mm), and rainfall erosivity (MJ mm (ha hr)$^{-1}$), respectively. $K$, $CL$, $SI$, $SA$, and $OC$ show soil erodibility (t ha hr (MJ ha mm)$^{-1}$), clay (%), silt (%), sand (%), and soil organic carbon (%), respectively. $C$ is the conservation factor and $\alpha$ and $\beta$ are constants (Ahmadi Mirghaed et al., 2018; Derakhshan-Babaei et al., 2021; Renard et al., 1996; Sharp et al., 2020; Sun et al., 2014; Wischmeier and Smith, 1978).

$$NDVI = (NIR - RED)/(NIR + RED) \tag{5}$$

$$SAVI = (1 + 0.5)(\frac{NIR - RED}{NIR + RED + 0.5}) \qquad (6)$$

$$EVI = 2.5 \times (\frac{NIR - RED}{NIR + 6 \times RED - 7.5 \times Blue + 1}) \qquad (7)$$

$$LAI = 0.56 \times \frac{NIR}{RED} - 0.83 \qquad (8)$$

where *NIR*, *RED*, and *Blue* represent the infrared, red, and blue bands of Landsat 8 images, respectively (Blinn et al., 2019; Huete, 1988; Liu and Huete, 1995; Rouse et al., 1974; Salas and Henebry, 2013).

**Table 1.** P factor values based on slope classes

| Class | Slope (%) | P factor |
|-------|-----------|----------|
| 1 | 3> | 0.6 |
| 2 | 3-9 | 0.5 |
| 3 | 9-12 | 0.6 |
| 4 | 12-15 | 0.7 |
| 5 | 15-20 | 0.8 |
| 6 | 20-25 | 0.9 |
| 7 | 25< | 1 |

*2.3. Sediment retention and sediment yield*

The sediment delivery ratio (SDR) model in InVEST was applied to investigate the ecosystem services of sediment retention (SR) and sediment yield (SY). This model operates based on the RUSLE method and receives information related to the digital elevation model, soil properties, land use, precipitation, and climate data in a raster format. It combines the data based on equation 9 to approximate soil erosion and calculates SR and SY using equations 10 and 11 (Sharp et al., 2020).

$$E_i = R_i \times K_i \times LS_i \times C_i \times P_i \qquad (9)$$

$$SR = E_i(1 - C_i P_i).SDR_i \qquad (10)$$

$$SY = \sum_{i=1}^{n} E_i \times SDR_i \qquad (11)$$

where, $E_i$, $R_i$, $K_i$, $LS_i$, $C_i$, and $P_i$ denote soil loss potential (t ha$^{-1}$yr$^{-1}$), rainfall erosivity (MJ mm (ha hr)$^{-1}$), soil erodibility (t ha hr (MJ) ha mm)$^{-1}$), slope length-gradient factor, landcover management factor, and land conservation factor, respectively. The SDR model shows the ratio of sediment yield in a region entering the rivers. This process is a function of the slope and downslope flow path for each pixel. This model first calculates the index of connectivity (IC) based on the following equations:

$$IC = \log_{10}(D_{up}/D_{dn}) \qquad (12)$$

$$D_{up} = \overline{CS}\sqrt{A} \qquad (13)$$

$$D_{dn} = \sum_i d_i / C_i S_i \qquad (14)$$

$$SDR_i = SDR_{max}/(1 + ex\,p\left(IC_0 - \frac{IC_1}{k_b}\right)) \qquad (15)$$

where $D_{up}$ and $D_{dn}$ respectively refer to components of up and down slopes. *C* and *S* respectively denote the average C factor and slope changes in the specific region. *A* is the area of the upstream slope (one pixel per square meter) and $d_i$ shows the average flow path length (from pixel *i* to the flow in meters) in the direction of the slope. $S_i$ and $C_i$ are the slope changes and C factor of pixel *i*, respectively. The upstream slope area and slope flow path are estimated using the D-infinity flow algorithm. $SDR_{max}$ or maximum SDR is defined as the maximum ratio of fine sediment that could enter the river flow. Without accurate information about the soil, its value is 0.8. $K_b$ and $IC_0$ are the calibration parameters that determine the sigmoid function SDR-IC relationship (Hamel et al., 2015; Mirghaed and Souri, 2023; Sharp et al., 2020; Woznicki et al., 2020). This study implemented different scenarios to evaluate SR and SY based on changes in the C factor in the InVEST software for each season in 2022.

*2.4. Statistical Analysis*

Geographically weighted regression (GWR) was employed to examine the relationship of sediment retention (SR) and sediment yield (SY) with the vegetation indices, *i.e.*, NDVI, SAVI, EVI, and LAI, for each season in 2022 in Arc GIS 10.7 at the sub-watershed level. GWR is a statistical method for modeling heterogeneous spatial relationships that assumes and analyzes the relationship between geographic variables in an unstable space. Spatial heterogeneity stipulates that there is a different relationship between the dependent and independent variables at each geographical point (Brunsdon et al., 1998; ESRI, 2016). Moreover, the region's sub-watersheds were categorized based on the dominant type of land use (forest, agriculture, and rangeland), and the one-way ANOVA test was used to find a significant difference of SR, SY and vegetation indices between the classified sub-watersheds.

**3. Results and discussion**

The results showed that 196301, 165883, 100849, 8735 and 195 ha of the watershed corresponded to the forest, agriculture, rangeland, built-up area, and waterbody,

respectively. The first three are the dominant land uses covering 98% of the region. Geographically, they include the central, northern and southern parts of the region, respectively. Figure 2 shows the maps of the R, K, LS, P and C factors in different seasons. The mean, minimum, and maximum values of the R factor were 307, 26 and 2141 (MJ mm (ha hr)$^{-1}$), respectively. Similarly, these values were 0.16, 0.12 and 0.27 for the K factor (t ha hr (MJ ha mm)$^{-1}$), 46, 0.02 and 171 for the LS factor and 0.84, 0.5 and 1 for the P factor, respectively. The mean C factor in spring, summer, autumn and winter were 0.17, 0.19, 0.24 and 0.30, respectively. Mirghaed and Souri (2023) also reported the R, K and C values of 6.3 to 1006 (MJ mm (ha hr)$^{-1}$), 0.09 to 0.5 (t ha hr (MJ ha) mm)$^{-1}$), and 0 to 2.1, respectively, for the Shoor River basin in the southwestern Iranian province of Khuzestan. For the Kan catchment

Tehran province, in the central Iran, Derakhshan-Babaei et al. (2021) found R and K values of 5.1 to 55.4 (MJ mm (ha hr)$^{-1}$) and 0.19 to 0.72 (t ha hr (MJ ha mm)$^{-1}$), respectively. Figures 3 and 4 indicate sediment retention (SR) and sediment yield (SY) in the region. Annually, 229 Mt of soil (471 t ha$^{-1}$ y$^{-1}$, on average) is retained in the watershed, while 5.2 Mt of soil (11 t ha$^{-1}$ y$^{-1}$, on average) is yielded. Mirghaed and Souri (2023) used InVEST to estimate the amount of SR and SY in the Shoor River basin in the Khuzestan province, southwestern Iran, at 3.8 Mt y$^{-1}$ (13.3 t ha$^{-1}$ y$^{-1}$) and 0.76 Mt y$^{-1}$ (2.7 t ha$^{-1}$ y$^{-1}$), respectively. The mean SR was estimated at 494, 487, 471 and 435 t ha$^{-1}$ in spring, summer, autumn and winter, respectively and similarly, the mean SY was estimated at 7.2, 8.4, 11.3 and 17.2 t ha$^{-1}$, respectively.
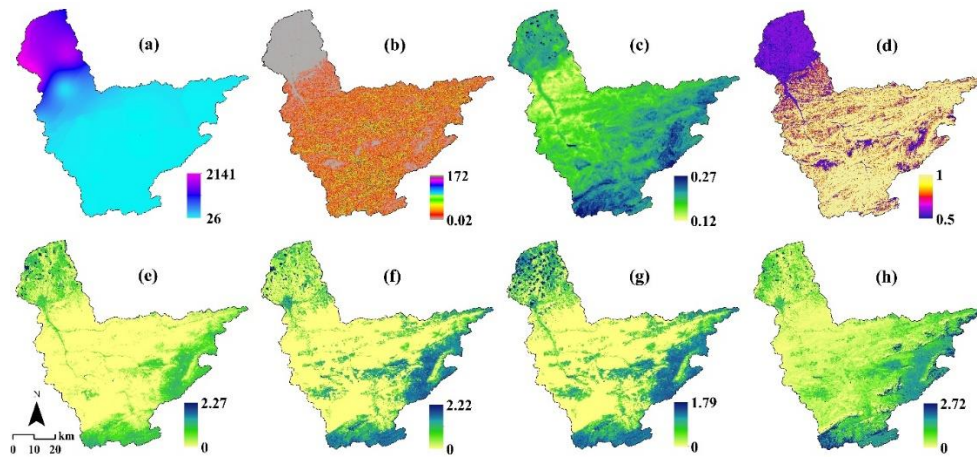


**Fig. 2.** Maps of (a) R factor (MJ mm (ha hr)$^{-1}$), (b) LS factor, (c) K factor (t ha hr (MJ ha mm)$^{-1}$) and (d) P factor alongside the maps of C factor in (e) spring, (f) summer, (g) autumn and (h) winter.
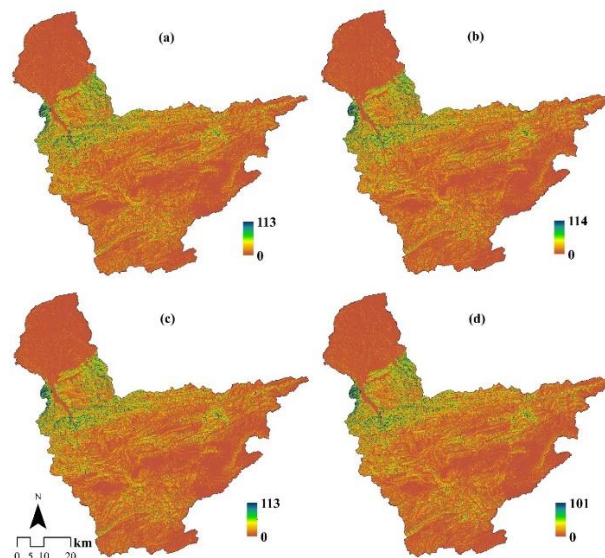


**Fig. 3.** Maps of sediment retention (t pixel$^{-1}$) in the study area in (a) spring, (b) summer, (c) autumn and (d) winter. The size of a pixel was 30 x 30m.
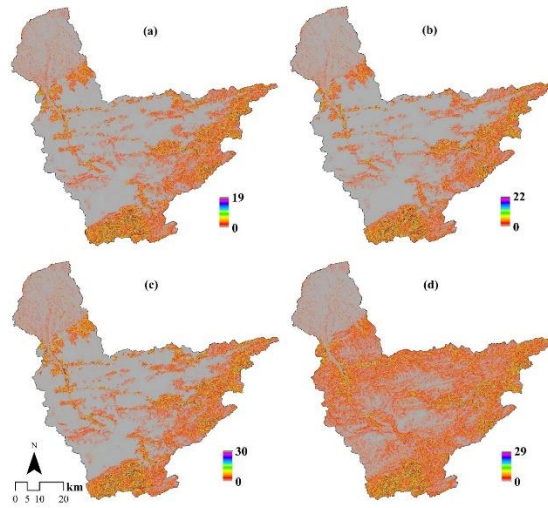
**Fig. 4.** Maps of sediment yield (t pixel$^{-1}$) in the study area in (a) spring, (b) summer, (c) autumn and (d) winter. The size of a pixel was 30 x 30m.

Table 2 illustrates the mean annual SR and SY per hectare for different land uses. The mean annual SR in forest, rangeland, agriculture and built-up areas were respectively 777, 200, 391 and 184 t ha$^{-1}$ in spring, 779, 171, 389 and 183 t ha$^{-1}$ in summer, 774, 158, 355 and 180 t ha$^{-1}$ in autumn, and 690, 133, 363 and 183 t ha$^{-1}$ in winter. Moreover, the mean annual SY in the aforementioned land uses was respectively 0.3, 22, 6.3 and 4.6 t ha$^{-1}$ in spring, 0.2, 28.2, 6.2 and 4.7 t ha$^{-1}$ in summer, 0.5, 32.3, 11.7 and 5.4 t ha$^{-1}$ in autumn and 11.1, 39.4, 12.2 and 5.3 t ha$^{-1}$ in winter. The geographic relationship between SR and the SAVI, NDVI, EVI and LAI indices in different seasons was investigated using the GWR analysis in Arc GIS 10.7 (Figure 5).

**Table 2.** The amount of sediment retention and sediment yield (t ha$^{-1}$) in each land use in different seasons during 2022

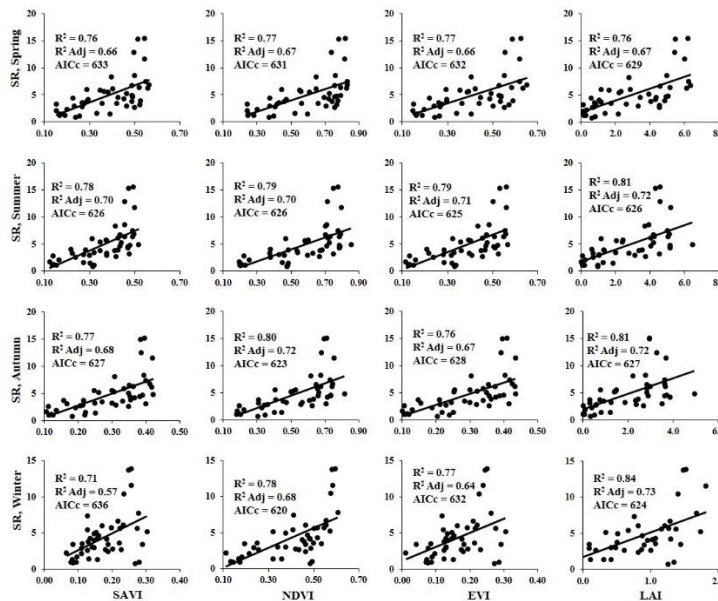| Season | Forest | | Rangeland | | Agriculture | | Built-up area | |
|---|---|---|---|---|---|---|---|---|
| | SR$^*$ | SY | SR | SY | SR | SY | SR | SY |
| **Spring** | 777 | 0.3 | 200 | 22.0 | 391 | 6.3 | 184 | 4.6 |
| **Summer** | 779 | 0.2 | 171 | 28.2 | 389 | 6.2 | 183 | 4.7 |
| **Autumn** | 774 | 0.5 | 158 | 32.3 | 355 | 11.7 | 180 | 5.4 |
| **Winter** | 690 | 11.1 | 133 | 39.4 | 363 | 12.2 | 183 | 5.3 |
| **Mean** | 755 | 3.0 | 166 | 30.5 | 375 | 9.1 | 183 | 3.8 |
| *SR: sediment retention, SY: sediment yield | | | | | | | | |



**Fig. 5.** Results of analyzing the relationship between SR: sediment retention (10×t ha$^{-1}$) with soil adjusted vegetation index (SAVI), normalized difference vegetation index (NDVI), enhanced vegetation index (EVI), and leaf area index (LAI) in all four seasons based on the GWR method.

The results confirmed that SR had a positive geographic correlation with all four indices having the coefficient of determination ($R^2$) of 0.76, 0.78, 0.77 and 0.77 with SAVI, 0.77, 0.79, 0.80 and 0.78 with NDVI, 0.77, 0.79, 0.76 and 0.77 with EVI and 0.76, 0.81, 0.81 and 0.84 with LAI, in spring, summer, autumn and winter, respectively. Figure 6 displays the relationship between SY and the SAVI, NDVI, EVI and LAI indices in different seasons. The results clarified that SY had an inverse correlation with all four indices having $R^2$ of 0.85, 0.80, 0.79 and 0.68 with SAVI, 0.86, 0.80, 0.79 and 0.80 with NDVI, 0.85, 0.81, 0.79 and 0.67 with EVI and 0.84, 0.81, 0.80 and 0.75 with LAI in spring, summer, autumn and winter, respectively. The geographic correlation of SR and SY with the aforementioned indices over four seasons is presented in Figure 7.
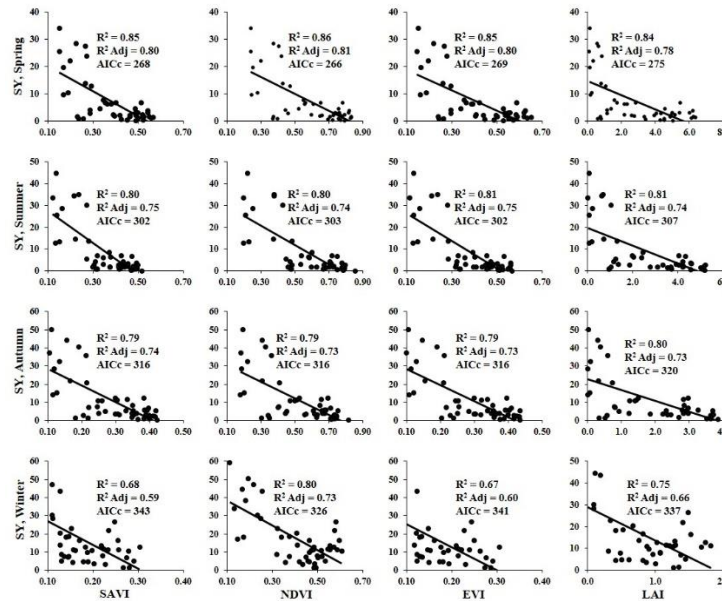


**Fig. 6.** Results of analyzing the relationship between SY: sediment yield (t ha$^{-1}$) with soil adjusted vegetation index (SAVI), normalized difference vegetation index (NDVI), enhanced vegetation index (EVI), and leaf area index (LAI) in all four seasons based on the GWR method.



**Fig. 7.** Results of analyzing the relationship between the mean of SR: sediment retention (10×t ha$^{-1}$) and SY: sediment yield (t ha$^{-1}$) with soil adjusted vegetation index (SAVI), normalized difference vegetation index (NDVI), enhanced vegetation index (EVI), and leaf area index (LAI) over four seasons based on the GWR method.
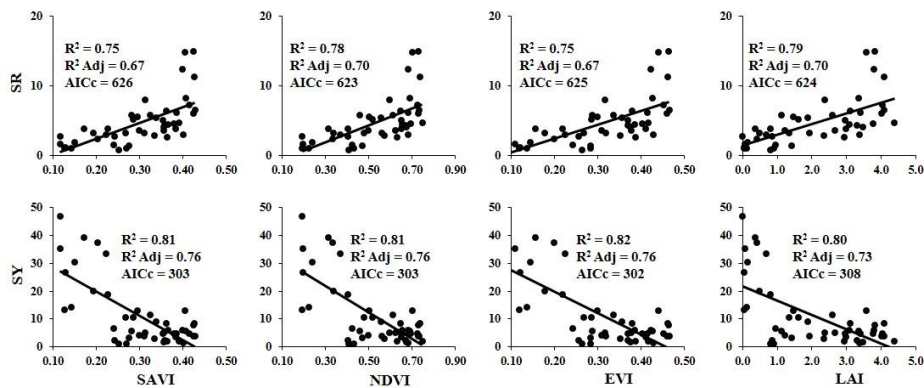
**Table 3.** Results of the one-way ANOVA

| Index* | F | P-value |
|---|---|---|
| SAVI | 96.5 | <0.01 |
| NDVI | 107.4 | <0.01 |
| EVI | 94.3 | <0.01 |
| LAI | 100.4 | <0.01 |
| SR | 11.4 | <0.01 |
| SY | 37.5 | <0.01 |

*SAVI: soil adjusted vegetation index, NDVI: normalized difference vegetation index, EVI: enhanced vegetation index, LAI: leaf area index, SR: sediment retention, SY: sediment yield

The results proved a positive correlation between the mean SR in four seasons and the SAVI, NDVI, EVI and LAI indices having $R^2$ of 0.75, 0.78, 0.75 and 0.79, respectively. Moreover, there was an inverse correlation between SY and the indices having $R^2$ of 0.81, 0.81, 0.82, and 0.80, respectively. The region's sub-watersheds were classified into three groups based on the dominant land use, indicating that the forest was dominant in 24 sub-watersheds in the central area, rangeland was dominant in 13 sub-watersheds in the southern area and agriculture was dominant in 9 sub-watersheds mostly in the north. Then, the one-way ANOVA was employed to evaluate the significance of the relationship between groups in terms of vegetation indices, SR and SY bringing the results in Table 3. Most of the precipitation in the Tajan watershed occurred in the north. Therefore, this area had the highest rainfall erosivity that gradually decreased from the north to the south. Most of the central and southern parts of the watershed had a diverse topography with steep slopes whereas the north is smooth and nearly flat. Therefore, the lowest slope length and steepness (LS factor) was observed in the north and the highest value was considered in the central and southern parts. The entire region had relatively low soil erodibility (K factor <0.28) due to adequate soil organic matter. However, the southern soils of the region had a higher erodibility than the other areas, whereas the central parts covered by various forest plants had the lowest. The highest P factor was seen in the central and southern parts, whereas the lowest value was observed in the north. This study mapped the C factor for each season in 2022 based on the NDVI. For all seasons, the results indicated that the C factor in the south of the watershed was higher than in other areas due to the lack of suitable vegetation whereas the value was the lowest in the central parts. Seasonally, the C factor in the study area varied based on the following trend: winter > autumn > summer > spring. This variability was the result of changes in vegetation from spring to winter. These results confirmed that geographic variations of R, K, LS, C and P factors across the region affect the conditions of sediment retention (SR) and sediment yield (SY). The highest SR was estimated in the central areas whereas the lowest occurred in the north and south of the watershed. The highest SY was seen in the southern areas and riverbanks, but it was lower in other parts of the

region. Adequate vegetation density in central areas leads to the entrapment of soil particles, SR and their reduced displacement, which thereby reduces SY. Low vegetation density, topography, and steep slopes lead to higher SY and lower SR in the southern areas of the watershed. In the northern parts, human activity and agriculture influence the reduction in SR and the increase in SY. Changing land uses, especially in riverbanks, has increased SY and reduced its retention in the region. Previous studies have also touched on the effect of vegetation density on SR and SY (Ahmadi Mirghaed et al., 2018; Hao et al., 2019; Tamire et al., 2022; Zhou et al., 2021). The region also showed different seasonal SR with the following trend: spring > summer > autumn > winter. However, the inverse was determined for SY. This is influenced by the reduction in vegetation density from spring to winter. Moreover, the higher frequency and intensity of precipitation in winter reduces SR and increases SY compared to other seasons. The estimated SR and SY in the watershed differed based on land use type. Regarding SR, land uses were ranked as follows: forest> agriculture> built-up area> rangeland and the ranking for SY was rangeland> agriculture> built-up area> forest. The ANOVA results also confirmed that the dominant land use type can have a significant effect on changes in SR, SY and vegetation cover. Adequate vegetation density in the region's forests had a positive influence on SR and SY. Furthermore, tree canopies prevent raindrops from directly affecting the soil and reduce rainfall erosivity, thereby reducing soil particle displacement and increasing SR. Most of the region's built-up areas are in the plains, which could explain its higher contribution to SR in comparison to rangelands and its lower contribution to SY in comparison to rangelands and agriculture. Mohammed et al. (2020) also stressed that vegetation can be an important factor in reducing rainfall erosivity and trapping sediments. The region's rangelands are scattered and have a diverse topography, which could increase SY and reduce SR. The results emphasized that in the aforementioned land uses, the highest and lowest SR occurred in spring and winter, respectively, whereas the inverse is the case for SY. Mirghaed and Souri (2023) also mentioned that the highest and lowest SR in the Shoor River basin in southwest Iran correspond to forests and built environments, respectively, whereas the highest

and lowest SY occurred in rangeland and forests, respectively. Woznicki et al. (2020) also proved that in steep erodible sites, forests lead to SR under heavy precipitation. The spatial correlation of SR with vegetation indices (NDVI, SAVI, EVI and LAI) in all four seasons was positive after evaluation using the GWR method and the changes in the correlation were minor in all cases ($0.76<R^2<0.84$). Nevertheless, on average, SR had a greater spatial correlation with LAI than the other indices. The results also showed that SY had an inverse correlation with the aforementioned indicators, and changes in correlation were higher ($0.67<R^2<0.85$). However, EVI had a greater spatial correlation with SY than the other indices. Seasonally, on average, there was a greater geographic correlation between SR and vegetation indices in summer whereas SY had a greater geographic correlation with the indices in winter. These results confirmed that vegetation changes in different seasons can affect soil SR and SY in the region with somewhat different spatial relationships in different seasons.

## 4. Conclusion

This study investigated sediment retention (SR) and sediment yield (SY) in the Tajan watershed in northern Iran based on the sediment delivery ratio (SDR) model in the InVEST software and analysis of seasonal vegetation changes during 2022. The results illustrated that maximum SR and SY were seen at the central and southern parts of the watershed, respectively. Forests had the highest SR while rangeland had the highest SY. Seasonally, spring and winter had the highest and lowest SR in the region, respectively, while the inverse was true for SY. The results confirmed that soil retention had a positive spatial correlation with the NDVI, SAVI, EVI and LAI indices while SY had a negative spatial correlation with them. Nevertheless, on average, SR had a greater spatial correlation with LAI and SY had a greater spatial correlation with EVI than the other indices. The spatial correlation between SR and SY was somewhat variable in different seasons. The results indicated that vegetation is a key factor in SR and SY in the study region and its seasonal effect could be somewhat different. These results can be essential for adopting the proper strategies and presenting helpful information to regional management to prevent erosion and protect the environment.

## References

Ahmadi Mirghaed, F., Souri, B., Mohammadzadeh, M., Salmanmahiny, A. & Mirkarimi, S.H., 2018. Evaluation of the relationship between soil erosion and landscape metrics across Gorgan Watershed in northern Iran. *Environmental monitoring and assessment,* 190, 1-14.

Babbar, D. et al., 2021. Assessment and prediction of carbon sequestration using Markov chain and InVEST model in Sariska Tiger Reserve, India. J*ournal of Cleaner Production*, 278, 123333.

Bagdon, B.A., Huang, C.H. & Dewhurst, S., 2016. Managing for ecosystem services in northern Arizona ponderosa pine forests using a novel simulation-to-optimization methodology. *Ecological Modelling*, 324, 11-27.

Bastos, M., Roebeling, P., Alves, F., Villasante, S. & Magalhaes Filho, L., 2023. High risk water pollution hazards affecting Aveiro coastal lagoon (Portugal)–A habitat risk assessment using InVEST. *Ecological Informatics*, 76, 102144.

Betrie, G.D., Mohamed, Y.A., Van Griensven, A. & Srinivasan, R., 2011. Sediment management modelling in the Blue Nile Basin using SWAT model. *Hydrology and Earth System Sciences*, 15, 807-818.

Blinn, C.E. et al., 2019. Landsat 8 based leaf area index estimation in loblolly pine plantations. *Forests*, 10, 222.

Brunsdon, C., Fotheringham, S. & Charlton, M., 1998. Geographically weighted regression. *Journal of the Royal Statistical Society*: Series D (The Statistician), 47, 431-443.

da Cunha, E.R. et al., 2022. Assessment of current and future land use/cover changes in soil erosion in the Rio da Prata basin (Brazil). *Science of The Total Environment*, 818, 151811.

Daneshi, A. et al., 2021. Modelling the impacts of climate and land use change on water security in a semi-arid forested watershed using InVEST. *Journal of Hydrology*, 593, 125621.

Derakhshan-Babaei, F., Nosrati, K., Mirghaed, F.A. & Egli, M., 2021. The interrelation between landform, land-use, erosion and soil quality in the Kan catchment of the Tehran province, central Iran. *Catena*, 204, 105412.

ESRI, 2016. ArcGIS Help Library. https://www.esri.com.

Fan, M., Shibata, H. & Chen, L., 2018. Spatial conservation of water yield and sediment retention hydrological ecosystem services across Teshio watershed, Northernmost of Japan. *Ecological Complexity*, 33, 1-10.

Fan, M., Shibata, H. & Wang, Q., 2016. Optimal conservation planning of multiple hydrological ecosystem services under land use and climate changes in Teshio river watershed, Northernmost of Japan. *Ecological indicators*, 62, 1-13.

Fenta, A.A. et al., 2021. Agroecology-based soil erosion assessment for better conservation planning in Ethiopian river basins. *Environmental research*, 195, 110786.

Gashaw, T. et al., 2021. Evaluating InVEST model for estimating soil loss and sediment export in data scarce regions of the Abbay (Upper Blue Nile) Basin: Implications for land managers. *Environmental Challenges*, 5, 100381.

Hamel, P., Chaplin-Kramer, R., Sim, S. & Mueller, C., 2015. A new approach to modeling the sediment retention service (InVEST 3.0): Case study of the Cape Fear catchment, North Carolina, USA. *Science of the Total Environment*, 524, 166-177.

Hao, R., Yu, D., Sun, Y. & Shi, M., 2019. The features and influential factors of interactions among ecosystem services. *Ecological Indicators*, 101, 770-779.

Hendi, E., Shamseldin, A.Y. & Melville, B.W., 2022. The effect of inlet width on the performance of sediment retention ponds in thermally induced flows. *Journal of Hydrology*, 606, 127377.

Hirave, P., Nelson, D.B., Glendell, M. & Alewell, C., 2023. Land-use-based freshwater sediment source fingerprinting using hydrogen isotope compositions of long-chain fatty acids. *Science of The Total Environment*, 875, 162638.

Hou, Y. et al., 2020. Ecosystem service potential, flow, demand and their spatial associations: a comparison of the nutrient retention service between a human-and a nature-dominated watershed. *Science of the Total Environment*, 748, 141341.

Huete, A.R., 1988. A soil-adjusted vegetation index (SAVI). *Remote sensing of environment*, 25, 295-309.

Li, M. et al., 2021. Evaluation of water conservation function of Danjiang River Basin in Qinling Mountains, China based on InVEST model. *Journal of environmental management*, 286, 112212.

Liu, H.Q. & Huete, A., 1995. A feedback based modification of the NDVI to minimize canopy background and atmospheric noise. *IEEE transactions on geoscience and remote sensing*, 33, 457-465.

MEA, 2005. Ecosystems and human well-being (Millennium Ecosystem Assessment). Island press United States of America.

Mirghaed, F.A. & Souri, B., 2023. Contribution of land use, soil properties and topographic features for providing of ecosystem services. *Ecological Engineering*, 189, 106898.

Mohammed, S. et al., 2020. Estimation of soil erosion risk in southern part of Syria by using RUSLE integrating geo informatics approach. Remote Sensing Applications: *Society and Environment*, 20, 100375.

Polasky, S. et al., 2012. Are investments to promote biodiversity conservation and ecosystem services aligned? *Oxford Review of Economic Policy*, 28, 139-163.

Redhead, J.W. et al., 2018. National scale evaluation of the InVEST nutrient retention model in the United Kingdom. *Science of the Total Environment*, 610, 666-677.

Regional Water Company of Mazandaran, 2023: Water resources report of Mazandaran province. www.mzrw.ir, (in persian).

Renard, K., Foster, G., Weesies, G., McCool, D. & Yoder, D., 1996. Predicting soil erosion by water: A guide to conservation planning with the Revised Universal Soil Loss Equation (RUSLE). *Agriculture handbook*, 703, 25-28.

Rouse, J.W., Haas, R.H., Schell, J.A. & Deering, D.W., 1974. Monitoring vegetation systems in the Great Plains with ERTS. *NASA special publication*, 351, 309.

Saha, S., Bera, B., Shit, P.K., Bhattacharjee, S. & Sengupta, N., 2022. Estimation of carbon budget through carbon emission-sequestration and valuation of ecosystem services in the extended part of Chota Nagpur Plateau (India). *Journal of Cleaner Production*, 380, 135054.

Salas, E.A.L. & Henebry, G.M., 2013. A new approach for the analysis of hyperspectral data: Theory and sensitivity analysis of the Moment Distance Method. *Remote sensing*, 6, 20-41.

Sharp, R. et al., 2020. InVEST 3.8.0 user's Guide. Stanford:The Natural Capital Project.

Shi, P. et al., 2022. Effects of grass vegetation coverage and position on runoff and sediment yields on the slope of Loess Plateau, China. *Agricultural Water Management*, 259, 107231.

Sun, W., Shao, Q., Liu, J. & Zhai, J., 2014. Assessing the effects of land use and topography on soil erosion on the Loess Plateau in China. *Catena*, 121, 151-163.

Tamire, C., Elias, E. & Argaw, M., 2022. Spatiotemporal dynamics of soil loss and sediment export in Upper Bilate River Catchment (UBRC), Central Rift Valley of Ethiopia. Heliyon, 8.

Tikuye, B.G., Gill, L., Rusnak, M. & Manjunatha, B.R., 2023. Modelling the impacts of changing land use and climate on sediment and nutrient retention in Lake Tana Basin, Upper Blue Nile River Basin, Ethiopia. *Ecological Modelling*, 482, 110383.

Wei, Q. et al., 2022. Temporal and spatial variation analysis of habitat quality on the PLUS-InVEST model for Ebinur Lake Basin, China. *Ecological Indicators*, 145, 109632.

Wei, S., Zhang, K., Liu, C., Cen, Y. & Xia, J., 2024. Effects of different vegetation components on soil erosion and response to rainfall intensity under simulated rainfall. *Catena*, 235, 107652.

Wischmeier, W.H. & Smith, D.D., 1978. Predicting rainfall erosion losses: a guide to conservation planning. Department of Agriculture, Science and Education Administration.

Woznicki, S.A. et al., 2020. Sediment retention by natural landscapes in the conterminous United States. *Science of the Total Environment*, 745, 140972.

Zhang, H. et al., 2021. Spatial distribution of carbon, nitrogen and sulfur in surface soil across the Pearl River Delta area, South China. *Geoderma Regional*, 25, e00390.

Zhou, M. et al., 2021. Evaluating combined effects of socio-economic development and ecological conservation policies on sediment retention service in the Qiantang River Basin, China. *Journal of Cleaner Production*, 286, 124961.

Zuazo, V.D. et al., 2008. Harvest intensity of aromatic shrubs vs. soil erosion: An equilibrium for sustainable agriculture (SE Spain). *Catena*, 73, 107-116.